Prepared for the National Institutes of Health
National Institute of Neurological Disorders and Stroke
Division of Fundamental Neurosciences
Neural Prosthesis Program
Bethesda, MD 20892

Unassisted Standing with Functional Neuromuscular Stimulation

NIH-NINDS-N01-NS-6-2351

Progress Report #6

Period Covered:
April 1, 1998 – June 30, 1998

Principal Investigator: Ronald J. Triolo, Ph.D.[1]
Co-Principal Investigators: Robert F. Kirsch, Ph.D.[2]
John A. Davis, Jr., M.D.[1]

Departments of Orthopaedics[1] and Biomedical Engineering[2]
Case Western Reserve University
Cleveland, OH 44106-4912

Co-Investigators: James J. Abbas, Ph.D.
University of Kentucky

Scott L. Delp, Ph.D.
Northwestern University

INTRODUCTION

The long-term goal of this contract is to develop methods to provide brace-free, energy efficient standing for persons with complete thoracic level spinal cord injuries via functional neuromuscular stimulation (FNS). The resulting system will resist reasonable disturbances and maintain balance automatically while allowing free use of the upper extremities to manipulate objects in the environment. These objectives are being addressed through an organized effort consisting of anatomical and dynamic modeling, control simulation and optimization, and experimental demonstration of new control structures. The work represents an active partnership between investigators at Case Western Reserve University (CWRU) and collaborators at Northwestern University (NU) and the University of Kentucky (UK).

Achieving independent, hands-free standing with FNS depends upon the development of an anatomically realistic and dynamic model of the lower extremities and torso. This model will be employed to conduct dynamic simulations and perform optimization procedures to investigate the theoretical behavior of various FNS control systems for providing automatic postural adjustments. Over the last quarter, substantial progress has been made in a) modeling the musculoskeletal anatomy of the trunk, b) performing experiments to validate both the general structure of the model and specific model parameter values, c) performing experiments to quantify the passive stiffness properties of the ankle, knee, and hip, and d) performing simulations to evaluate the feedforward control of standing by FNS. This report summarizes these results and their relationship to the overall goals of the contract.

III. PROGRESS THIS REPORTING PERIOD

Progress this reporting period was made primarily in the following areas: 1) anatomical modeling of the torso, 2) biomechanical modeling and simulation, 3) feedforward control of standing by FNS.

A. Anatomical Modeling of the Torso

A third set of dissection experiments was performed by the NU investigators on a cadaver specimen to analyze trunk muscles in detail and determine their architectural and morphometric parameters. A medium sized male specimen was obtained for the study. The skin and fascia from the dorsal surface were removed. The *trapezius* and *latissimus dorsi* were reflected to expose the columns of the erector spinae. The *multifidus* was removed to expose the *quadratus lumborum* muscle. The *rectus abdominus* was dissected from the ventral side. The skin, fascia, and the rectus sheath were removed to expose the *rectus abdominus*. Photographs and measurements were taken from the detached muscles before the muscles were removed and fixed in formalin, and markers were placed on key attachment locations according to the same protocol used for the first specimen as described in Quarterly Progress Reports 3 & 4. Detailed analysis to measure fiber alignment, fiber length, and sarcomere length will be performed during the next reporting period. The muscle measurements made during the dissection are listed in Table I.

Variation of muscle parameters from one subject to another is a major concern in modeling a muscle's force generating capacity. For this reason, we plan to measure muscle parameters from at least one more specimen (for a total of at least 4 specimens) in order to determine the range of values for each of the muscle parameters.

In summary, over the past year we have a) scaled a digitized representation of the vertebral column, b) compared antrhopometric parameters of each vertebra with data published in the literature, c) integrated the scaled representation of the spine into the existing lower extremity model, d) verified the overall model by comparing selected anthropometric parameters with published data, e) defined preliminary models of the spinal muscles based on anatomy texts and preliminary cadaver studies, f) completed a preliminary comparison of muscle moment arms with published CT/MRI data, g) harvested trunk muscles from three cadaver specimens, h) measured architectural and morphometric parameters for each muscle, and i) refined the preliminary model of the muscles based on the detailed analysis of the two specimens.

Muscle	Musculo-tendon length (cm)	Pennation Angle (degrees)
Quad. Lumb. (proximal)	11.5	5 - 10
Quad. Lumb. (distal)	10.0	0 - 5
Spin. Thoracis	26.0	15
Long. Thoracis	43.0	20
Illioc. Thoracis	40.5	10
Rectus Adb.	42.0	0

Table I: Muscle dissection measurements obtained from specimen 3.

B. Biomechanical Modeling and Simulation

Over the past 3 months, we have made substantial progress in two areas related to biomechanical modeling and simulation. Specifically, progress has been made in developing experimental techniques for validating the overall structure of the model and in developing experimental techniques to measure passive joint properties so that they can be incorporated into a subject-specific model.

In previous reports we described the development of a dynamic, three-dimensional, closed-chain model of the two human lower extremities and demonstrated the feasibility of using it to perform control simulations. The structure of this model is based upon detailed anatomical studies, segment mass properties can be adjusted for individual subjects, and Hill-type dynamic muscle models are used to represent muscle force generation. However, the overall capability of this model to reflect actual human movement properties has not been tested. Over the last three months we have therefore begun a set of experiments to validate the basic structure of the model,

using able-bodied human subjects and generic able-bodied model parameter values. Future experiments will be required to estimate subject-specific parameters in individuals SCI.

A second experimental protocol has also been developed over the past 3 months to measure the passive forces and moments developed by the joints and muscles of the lower extremities and pelvis during movements. The passive stiffnesses developed at these joints depend upon the state of the joint capsules and ligaments, as well as the connective tissues within the muscles. These properties are likely to be different in able-bodied and spinal cord injured individuals, and will likely vary significantly within the SCI population. These properties can be beneficial (e.g., provide joint stabilization) or detrimental (e.g., prevent a desirable upright standing posture). We have therefore developed experimental paradigms for measuring these properties at the ankle, knee, and hip. Initial experimental results presented here deal with the level of detail required for a model of passive tissue properties.

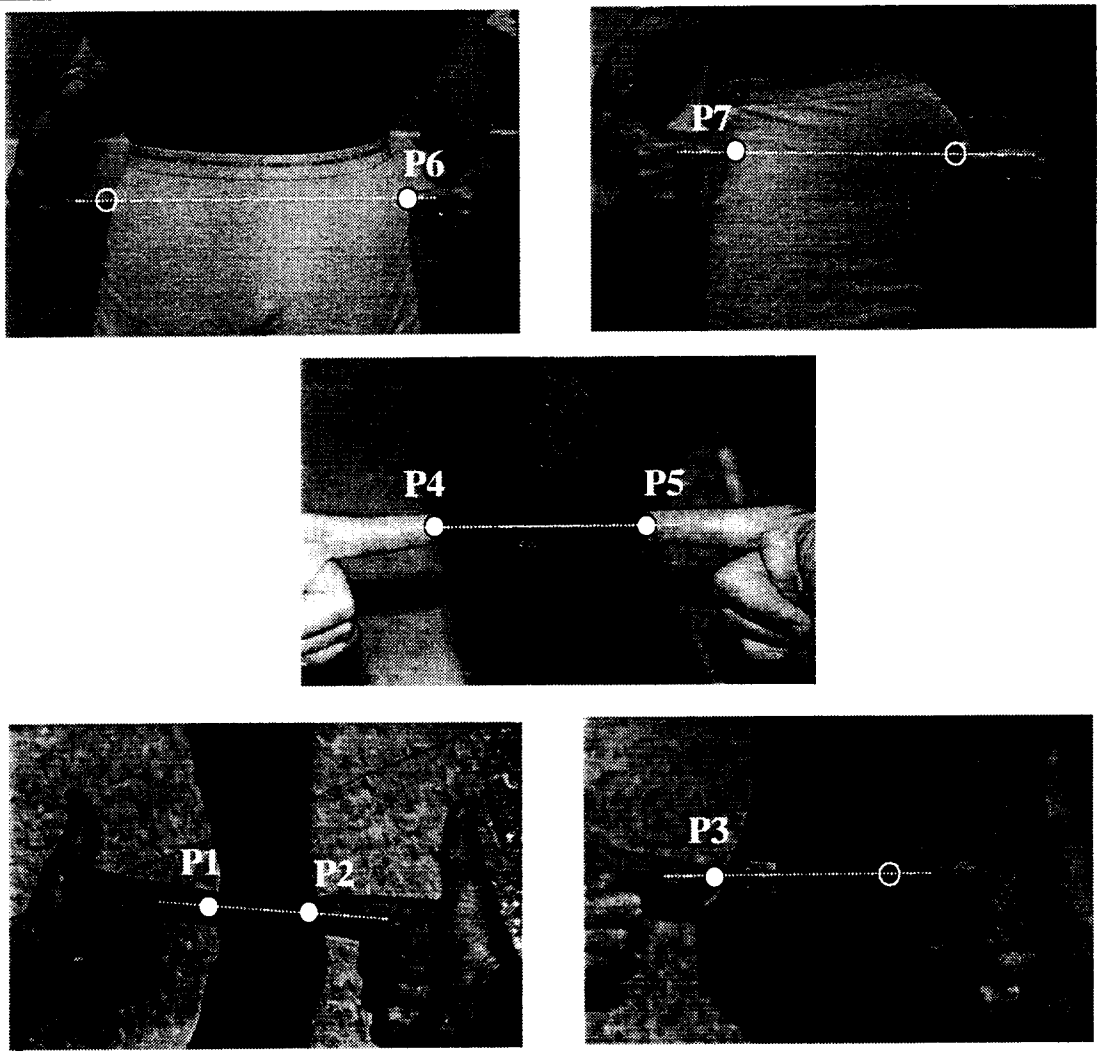

Figure 1: OptoTrak IRED's attached to body segments. The 3-D coordinates of the IREDs are used to define body-embedded local reference frames and to determine their orientations with respect to the global frame.

B. Model Validation

We previously reported our initial effort to prepare the experimental procedures and laboratory hardware and software required to evaluate global performance of the dynamic, three-dimensional, closed-chain model of the human lower extremities and pelvis simulating bipedal standing. The current reporting period has been dedicated in large part to conducting validation tests. After three pilot studies, a successful experiment was performed on one able-bodied volunteer. A complete set of 3-D kinematics, EMG signals, and ground reaction forces were collected for three body posture motions, five trials each. Preliminary results of individualizing the bipedal standing model, ground reaction force analysis, and EMG signal analysis are summarized in this report.

*1. **Individualization of the bipedal standing model:*** The kinematic model of bipedal standing is defined by segment lengths, joint axes, and body segment orientation using body-embedded reference frames and global reference frame. Each individual has personalized body dimensions. It is essential that the standing model be individualized accordingly before running forward dynamic simulations. In the validation experiment, an OptoTrak motion analysis system (Northern Digital, Inc.) was used to measure segment lengths, joint axes, and body segment orientations. Sixteen landmarks were used to define joint centers and axes. The specific locations of seven landmarks on the left leg are illustrated in Fig. 1. Landmark P1 and landmark P2 were pointed to the lateral and medial malleolus, respectively. Landmark P3 was pointed to the most inferior, lateral point on the posterior surface of the calcaneus. Landmark P4 and landmark P5 were pointed to the lateral and medial femoral epicondyles, respectively. Landmark P6 and its corresponding landmark on the right leg were pointed to the centers of left and right femoral heads, which constitute the hip joint axis of flexion/extension. Landmark P7 and its corresponding landmark on the posterior surface were pointed to the center of left femoral head and constitute the hip joint axis of abduction/adduction. One additional landmark P8 was placed on the top of acromioclavicular joint. Particular attention was paid to ensure these joint axis definitions were consistent with Delp et al. (1990) and the SIMM package (MusculoGraphics, Inc.).

For each body segment, a right-handed, orthogonal, anatomically-based reference frame was constructed based on landmark coordinates. The shank reference frame has its origin at the midpoint between the lateral (P1) and medial (P2) malleolus with axis directions defined as

$$\overline{Y}^S = \overline{P}_m^T - \overline{P}_m^S$$
$$\overline{X}^S = \overline{Y}^S \times (\overline{P}_1 - \overline{P}_m^S)$$
$$\overline{Z}^S = \overline{X}^S \times \overline{Y}^S$$

where $\overline{P}_m^T$ is the knee joint center, and $\overline{P}_m^S$ is the midpoint of the medial and lateral malleolus. The superscripts S and T denote to the shank and thigh segments, respectively.

The thigh reference frame has its origin at the midpoint between the lateral (P4) and medial (P5) femoral epicondyles with axis directions defined as

$$\overline{Y}^T = \overline{P}_m^P - \overline{P}_m^T$$
$$\overline{X}^T = \overline{Y}^T \times (\overline{P}_4 - \overline{P}_m^T)$$
$$\overline{Z}^T = \overline{X}^T \times \overline{Y}^T$$

where $\overline{P}_m^P$ is the hip joint center, and $\overline{P}_m^T$ is the midpoint of the medial and lateral femoral epicondyles. The superscripts P denotes to the pelvis segment.

The pelvis reference frame has its origin at the femoral head center, which was calculated based on landmark coordinates. Three axis directions of the reference frame are defined as

$$\overline{Y}^P = \overline{P}_m^P - \overline{P}_m^T$$
$$\overline{X}^P = \overline{Y}^P \times (\overline{P}_6 - \overline{P}_m^P)$$
$$\overline{Z}^P = \overline{X}^P \times \overline{Y}^P$$

In the anatomical position, axis X points anteriorly, axis Y points superiorly, and axis Z points laterally. All the body-embedded reference frames have the same initial orientation.

Segment lengths of the subject were calculated based on landmark coordinates: $L_{shank} = 433.0\,(mm)$, $L_{thigh} = 491.6\,(mm)$, and $L_{pelvis} = 207.6\,(mm)$.

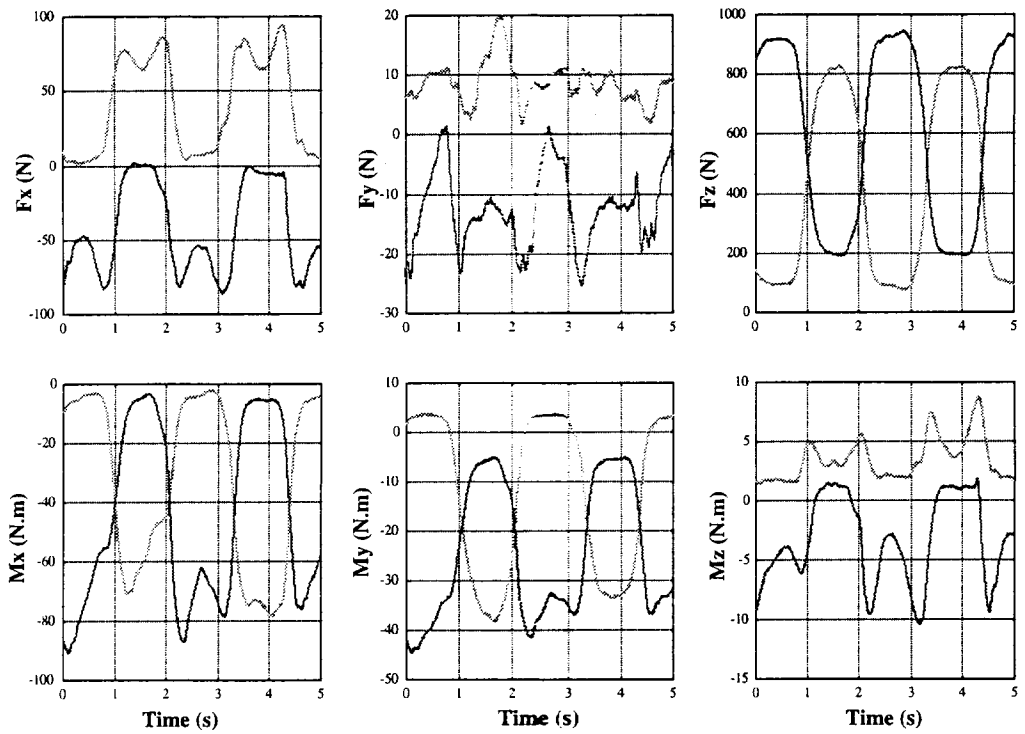

Figure 2: Ground reactions to body posture transfer (mainly) in the frontal plane. Heavy and light lines show the reaction forces and moment at the right force plate and left force plate, respectively.

*2. **Ground Reaction Forces:*** Two force plates with strain gauge transducers (AMTI, Inc.) were used to collect ground reaction forces and moments in the tests. Each plate gave three force (F_x, F_y, F_z) and three moment (M_x, M_y, M_z) components. Axis X points laterally; axis Y points anteriorly; and axis Z points vertical downward. The signals were amplified (2000x), low-pass filtered at $10.5Hz$, and sampled at $1000Hz$. The voltage signals were then converted to

force and moment signals according to factory-calibrated sensitivity matrices. The force plates were switched on 30 minutes prior to the test in order to stabilize the plates.

While the subject stood quietly on two force plates, the summation of two vertical force components was approximated equal to his body weight, which is $182lb$ (=$809.6N$). The summation of horizontal components in either X or Y direction is approximately zero. When the subject shifted his body posture, the two force plates recorded the dynamic ground reaction forces and moments. One representative set of the force and moment data is plotted in Fig. 2. During this trial, the subject shifted his body posture mainly in the frontal plane. The vertical force components clearly showed that he switched body weight between two legs when he shifted his body posture. The minimum values of vertical force components are greater than zero, which means that the subject did not lift his feet during the trial. The dynamic range of vertical force on each force plate is approximately 100% about the nominal value of half his body weight (=$404.6N$). In addition, the summation of vertical forces is at times greater than his body weight due to dynamic effects of posture sway. The changing pattern of forces and moments indicated that the body posture swayed at about $1Hz$.

3. Lower Extremity Muscle Activities: The activities of sixteen lower extremity muscles, eight from each leg, were monitored in the experiment using surface EMG electrodes. Based on relative muscle strength analysis (See Progress Report #4) and accessibility of surface electrodes, the selected muscles and their major joint functions are:

(1) Tibialis Anterior (TA): dorsiflexes the ankle joint and assists inversion of the foot;

(2) Medial Gastrocnemius (MG): flexes the ankle and knee joints;

(3) Semimembranosus (SM): flexes the knee joint and extends the hip joint;

(4) Vastus Lateralis (VL): extends the knee joint;

(5) Rectus Femoris (RF): extends the knee joint and flexes the hip joint;

(6) Gluteus Maximus (GM): assists in extension of the hip joint;

(7) Adductor Magnus (AM): adducts the hip joint;

(8) Gluteus Medius (GM): assists hip abduction, and medially rotates the hip joint (upper fibers) or laterally rotates the hip joint (lower fibers).

Bipolar silver-silver chloride, disposable recording electrodes were placed over the sixteen lower extremity muscles. A ground electrode was placed over the left medial tibial plateau. The EMG signals were amplified (5000x), lower-pass filtered at $200Hz$ by analog Bessel filters (IOtech, Inc.), and collected by 64-channel A/D board (National Instruments, Inc.). The subject was asked to perform maximum isometric contractions of each of the sixteen muscles before the experiment to record maximal EMG values for each muscle. The EMG signals were initially examined using an oscilloscope to ensure that the cross-talk between muscles was minimal. The recorded EMG signals were digitally full-wave rectified and numerically filtered by a 6^{th}-order Butterworth low-pass filter at a cutoff frequency of $3Hz$ in order to obtain the linear envelop of the signals (Winter, 1990).

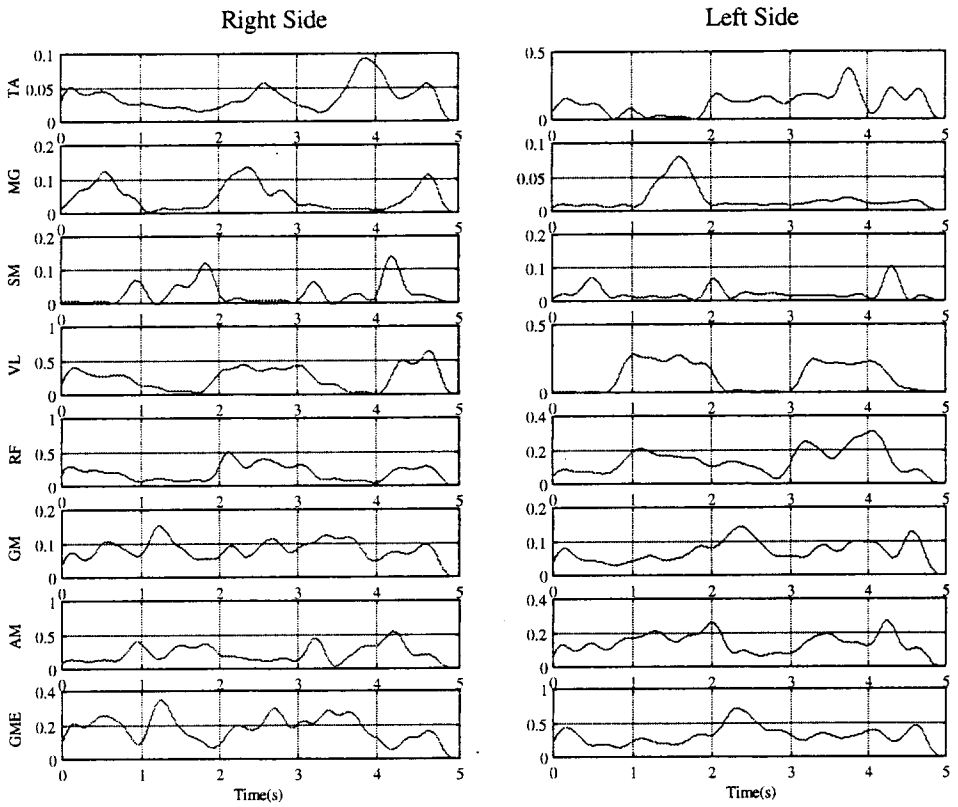

Figure 3: EMG responses to body posture transfer (mainly) in the frontal plane. The clear on-off patterns show there is close collaboration among the lower extremity muscles in order to achieve body posture shift and maintain balance.

One representative set of EMG responses is illustrated in Fig. 3, where each individual EMG signal has been normalized by its maximum isometric value. As stated in previous section, the postural sway during this trial occurred mainly in the frontal plane, with a sway frequency of approximately $1Hz$. The figure shows that there is close and efficient collaboration among the lower extremity muscles during the body sway. For example, when a muscle from one leg is active, its counterpart on the opposite leg is usually inactive. Antagonistic muscle pairs at the ankle and knee joints show quite low co-contraction levels. Antagonistic muscle pairs at the hip joints, however, have relatively large co-contraction levels. In addition, muscle activation levels at the ankle and knee joints were smaller than those at the hip joints, which indicates that the control strategy being used during the test can be comparable to so-called "hip strategy" (Horak et al., 1990).

4. Summary and immediate plans: The data recorded in the experiments described in the previous 3 subsections (i.e., lower extremity and pelvis kinematics, ground reaction forces, and muscle EMG signals) will be used in the next period to evaluate the overall performance of the model. Inverse simulations with the model will predict muscle force levels needed to reproduce the observed movements. These simulated forces will in turn predict ground reaction forces,

which will be compared to those measured experimentally. Furthermore, the patterns of simulated forces required across the various muscles during various sway-type movements will be compared to the

References:

1. Delp, S. L., Loan, J. P., Hoy, M. G., Zajac, F. E., Topp, E. L., and Rosen, J. M., 1990, "An interactive, graphics-based model of the lower extremity to study orthopaedic surgical procedures," *IEEE Trans. Biomed. Eng.*, 37: 757-767
2. Winter, D. A., 1990, "Biomechanics and Motor Control of Human Movement," 2nd Edition, *John Wiley & Sons*, Inc, pp. 191-212
3. Horak, F. B., Nashner, L. M. and Diener, H. C., 1990, Postural strategies associated with somatosensory and vestibular loss, *Exp. Brain. Res.*, **82**: 167-177

C. Adjusting model passive stiffness parameters for chronic SCI and FNS: the effects of joint preconditioning

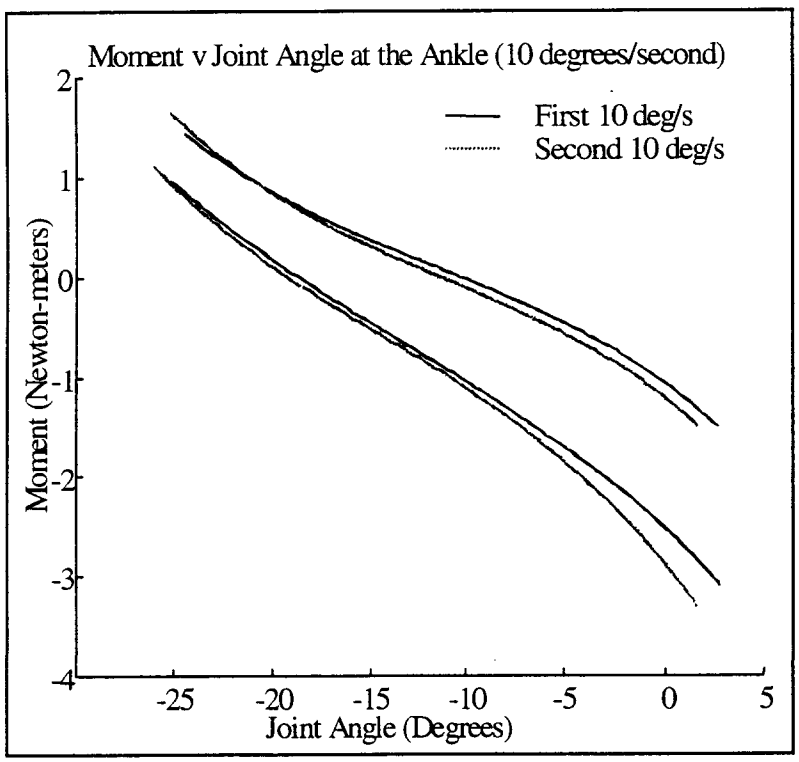

Figure 4: The effect of using a 30 min. interlude to place the ankle in an unconditioned state. After 30 min. of inactivity, the first cycle of the second test is very similar to the first cycle of the first test.

The passive joint properties of able-bodied individuals have been evaluated in a number of previous studies, although in almost every case the measurements have been made after the joint has been *preconditioned.* Preconditioning consists of the joint being externally moved throughout its range of motion several times in sequence. These movements significantly reduce the complexity of force responses seen from a joint that has been at rest, where stiffness is usually higher and a significant hysteresis is observed (i.e., the force at a given position is different depending upon which direction the joint has moved to reach that

which will be compared to those measured experimentally. Furthermore, the patterns of simulated forces required across the various muscles during various sway-type movements will be compared to the

References:

1. Delp, S. L., Loan, J. P., Hoy, M. G., Zajac, F. E., Topp, E. L., and Rosen, J. M., 1990, "An interactive, graphics-based model of the lower extremity to study orthopaedic surgical procedures," *IEEE Trans. Biomed. Eng.*, 37: 757-767
2. Winter, D. A., 1990, "Biomechanics and Motor Control of Human Movement," 2nd Edition, *John Wiley & Sons*, Inc, pp. 191-212
3. Horak, F. B., Nashner, L. M. and Diener, H. C., 1990, Postural strategies associated with somatosensory and vestibular loss, *Exp. Brain. Res.*, **82**: 167-177

C. Adjusting model passive stiffness parameters for chronic SCI and FNS: the effects of joint preconditioning

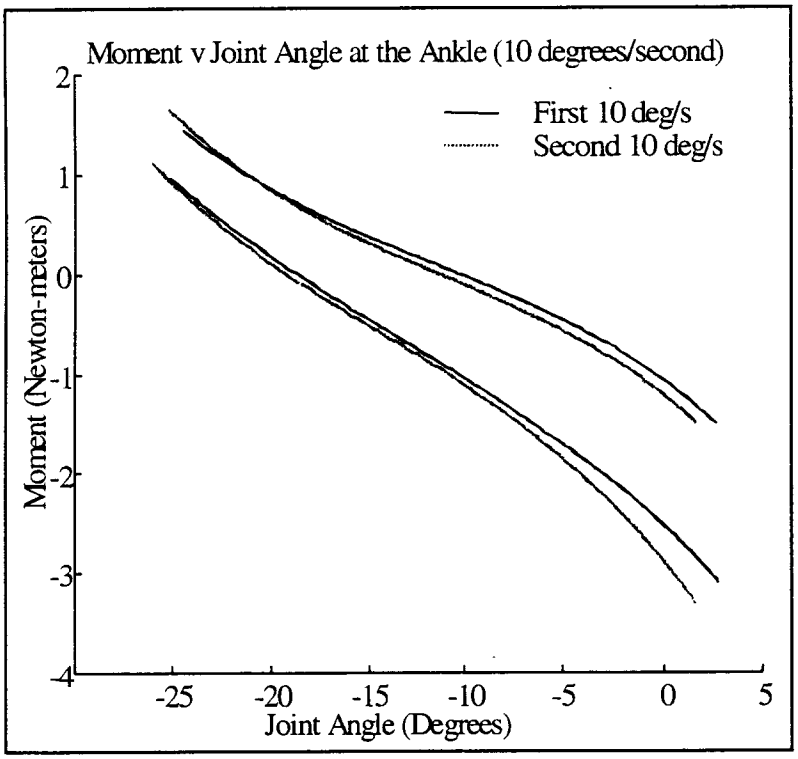

Figure 4: The effect of using a 30 min. interlude to place the ankle in an unconditioned state. After 30 min. of inactivity, the first cycle of the second test is very similar to the first cycle of the first test.

The passive joint properties of able-bodied individuals have been evaluated in a number of previous studies, although in almost every case the measurements have been made after the joint has been *preconditioned.* Preconditioning consists of the joint being externally moved throughout its range of motion several times in sequence. These movements significantly reduce the complexity of force responses seen from a joint that has been at rest, where stiffness is usually higher and a significant hysteresis is observed (i.e., the force at a given position is different depending upon which direction the joint has moved to reach that

position). Preconditioning a joint is known to reduce passive forces required to hold a joint at a particular location and to reduce or even eliminate the hysteresis. For able-bodied individuals the practice of preconditioning may be appropriate since previous movements in their daily activities often will have already preconditioned the joints naturally. However, this practice may not be appropriate for individuals with spinal cord injuries because their joints are often immobile for long periods of time. Consequently, their joints will be in an unconditioned state when they attempt to stand. In developing a passive moment model for individuals with SCI, it is thus important to answer the following two questions about conditioning: 1) How much does the passive moment differ between a preconditioned and an unconditioned joint? and 2) Are these differences significant enough to be included in the model?

A key aspect of this part of the project is to determine what preconditioning effect size is significant to our goal of providing unassisted standing. In this application, the main objective is to provide an adequate amount of active moment at each of the lower extremity joints for an individual to stand. Passive moments will be in opposition to the active moments during the sit-to-stand transition but could be helpful once the standing position is obtained. Furthermore as a percentage of the total moments encountered during a sit-to-stand transition, passive moments are usually small in able-bodied individuals. Thus, if conditioning greatly affects the passive moment measured, conditioning could still be insignificant if the passive moment is only a small percentage of the total moment. Thus, the relevant question to be addressed here is whether preconditioning effects significantly impact the amount of active moment needed to complete the sit-to-stand transition.

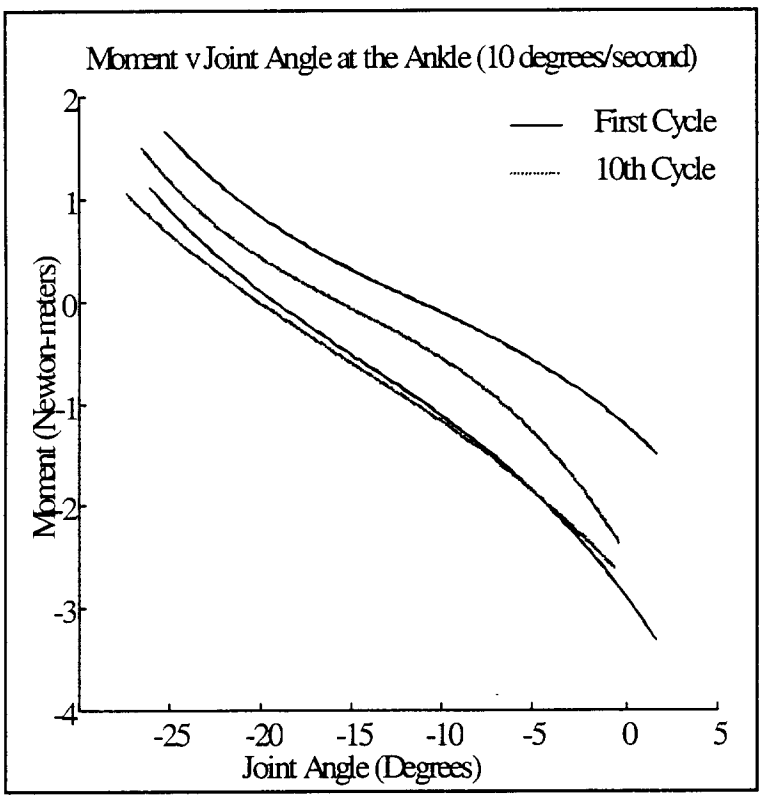

Figure 5. The effect of preconditioning on the passive moment at the ankle. After cycing the ankle through its range of motion 10 times, the magnitude of the passive moment decreases.

To answer these questions, we have begun to measure the effects of conditioning at the ankle joint. The protocol used to measure the effects of conditioning consisted of putting the subject's ankle in an unconditioned state and then passively cycling it through a range of motion 10 times to determine the amount of decline in its

passive moment response. A KinCom robotic dynamometer was used to cycle the joint isokinetically at 10 degrees/second. To obtain an unconditioned state the subject's ankle was attached to the dynamometer and held in a fixed position for 30 minutes before the testing began. The ankle was tested a total of 3 times with the ankle fixed for 30 minutes between each test. During each of the last two tests the ankle was cycled 20 times. Repeating the tests with 30-minute interludes allowed us to evaluate whether 30 minutes was enough time for the ankle joint to revert to an unconditioned state. Using 10 cycles for one test and 20 cycles for another test aided us in determining the necessary number of cycles needed for the ankle to become conditioned.

Figure 4 shows the effects of the 30-minute interlude. The solid curve represents the moment responses of the first cycle of the first test. The top curve represents the response as the ankle is moved from dorsiflexion to plantarflexion. The bottom curve represents the response during the second half of the cycle when the ankle moves from plantarflexion to dorsiflexion. The hysteresis of the passive properties is seen as the different forces obtained at a given position depending on whether the joint was being dorsiflexed or plantarflexed. The dotted curve shows the moment response for the first cycle of the second test (after 30 min. of inactivity). The similarities between the two sets of curves suggest that 30 minutes is long enough for the ankle to revert to an unconditioned state.

The curves of **Figure 5** show the effects of conditioning. The solid curve represents the moment response of the first cycle and the dotted curve represents the moment response of the tenth cycle. As in **Figure 4** the top curves represent the movement from dorsiflexion to plantarflexion and the bottom curve curves show the response from plantarflexion to dorsiflexion. The effects of conditioning are seen by the decreased amount of hysteresis between the top and bottom curves of the tenth cycle. The decrease in the hysteresis illustrates that the joint would need less active moment to overcome the passive moment once the joint has been conditioned.

Comparing the magnitudes of the unconditioned and conditioned responses for this subject, however, it was found that the maximum difference was approximately 1 N-m. Although 1 N-m is a significant change in the passive properties of this subject, a 1 N-m change in the passive moment is not very significant when comparing the passive moment to the active moment. Active moments at the ankle during the sit-to-stand transition are in the range of 12-15 N-m, so a change of 1 N-m is less than a 10% change. Thus, it appears that a simple model which does not include the nonlinear viscoelastic properties of the unconditioned joint will be sufficient for the model being developed here.

The results presented above are from a single able-bodied subject, however. Additional tests will be performed on both able-bodied and SCI individuals to more fully validate these conclusions. Once the issue of preconditioning is resolved, standard passive moment measurements will begin on both able-bodied and SCI subjects. Using the empirical data, model components will be developed to describe the passive moments at each of the lower extremity joints. The passive moment model will be incorporated into the overall biomechanical model and the significance of the passive contributions during standing and during the sit-to-stand transition will be examined in simulation. We will then proceed to examine the active contractile properties of stimulated paralyzed muscle in an effort to continue refinement of the model.

D. Feedforward Control of Standing by Functional Neuromuscular Stimulation

In this contract period, the UK subcontract has focused efforts on 1) using models to study the effects of varying model parameters and the effects of co-stimulation parameters on control system performance, 2) continued development of software for real-time controller implementation and for simulation, and 3) preparing human subjects for standing control experiments. Each of these developments is briefly outlined below.

*1. **Model-based studies:*** In this contract period we have utilized a musculoskeletal model to study the sensitivity to various model parameters and to study the effects of varying the co-stimulation map parameters on control system performance. This work has been submitted as an abstract to the upcoming Biomedical Engineering Society meeting and the student working on the project has submitted a supplemental paper to the student paper competition for the meeting. This paper is provided as an appendix. Briefly, the results of that study indicate that postural stability may be most highly sensitive to muscle torque-angle dependence (i.e. muscle force-length dependence). In a series of simulations, the study demonstrated that the response to disturbances was highly influenced by that model parameter. The second result of these studies was that although co-stimulation levels provide stability by stiffening the system, the gains to be achieved may have diminishing returns and the cost of excessive co-stimulation may include a poor transient response as well as increased energy expenditure. The implications from these results are that we should assess muscle torque-angle dependence as accurately as possible and that we should carefully assess the sensitivity of control system performance to this parameter. Secondly, selecting an appropriate co-stimulation level is essential, as anticipated, and that allowing the user to adjust these levels on-line may be a very useful feature.

*2. **Software development for simulation and experimental studies:*** We have continued our efforts at developing the software that is required for both the simulation and experimental studies. In this contract period we have made substantial progress in the development and implementation of the adaptive control algorithm that will be used in simulation studies and real-time control. The control algorithm, which had previously been implemented in the Matlab environment, has now been written in 'C' and is currently being interfaced with SIMM/SDFAST code for simulation studies and interfaced with LabVIEW software for real-time control. In other work, we have completed the development of LabVIEW-based software that will be used in studies to evaluate candidate user input devices and in the real-time control system.

*3. **Preparing human subjects for standing experiments.*** Two subjects with spinal cord injury have been recruited into our research program and have been undergoing an exercise protocol to build strength and endurance of the extensor muscles. The two subjects both have thoracic-level injuries (T-4 male, T-11 female) and have thus far been enthusiastic participants. Note that these subjects have been enrolled in the research program under the IRB approval for a different project, but they have verbally agreed and are enthusiastic about this standing project. As soon as they have developed the required strength and endurance for standing and the NPS-4 stimulator for this study is functional, they will be officially enrolled in the contract sponsored program and standing experiments will be initiated. Thus far, both of these subjects have made steady progress, although it has been slower than expected. The response of the quadriceps has gone from trace contractions to the point where they can repeatedly lift their swinging lower leg

while seated with weights attached to their ankles. They have also made progress in developing hip extensor strength.

4. Summary and immediate plans: In this contract period we have obtained some important results from the simulation studies and we have made progress towards initiating experimental evaluation of the control systems. In the upcoming contract period, we expect that we will be ready to begin standing experiments. The two essential tasks towards this goal will be to build enough strength and endurance in our two subjects and to interface the control system software with our real-time systems. The model-based efforts will focus on characterizing the effects of co-stimulation in a more complex standing model and to continue the evaluation of the adaptive control scheme in that model.

The effects of co-stimulation map parameters on FNS system performance

Xia Zhang[1], James J. Abbas[1] and Ronald J. Triolo[2]

[1]University of Kentucky, Center for Biomedical Engineering, Lexington, KY, [2]Case Western Reserve University, Department of Orthopedics, Cleveland, OH

Abstract

Many Functional Neuromuscular Stimulation (FNS) systems use a co-stimulation map to direct a single control signal to several muscles and to compensate for muscle non-linearities. The goals of this study were to investigate the effects of co-stimulation map parameters on control system performance and to determine which system components had the strongest effects on controller performance. A feedback controller was used with a co-stimulation map to control upper body movements in the sagittal plane during stance by stimulating paralyzed hip abductor muscles. A modified Hill-type muscle model and a single-segment inverted pendulum skeletal model were used in the computer simulation. Performance was evaluated using the system response to small amplitude position changes. Our results indicate that controller performance depends strongly on muscle length-dependence and can be improved by proper selection of co-stimulation map parameters.

Introduction

Functional Neuromuscular Stimulation (FNS) has been developed as a rehabilitative technology for people with neurological disorders. A musculoskeletal model of a FNS system (Fig 1) includes two muscles acting on a single, planar skeletal segment. Fixed parameter, open-loop control schemes have most often been used, but feedback (dotted line) has been used to improve performance. The co-stimulation map (Fig 2) has been used to direct a single control signal to several muscles [2,3,4]. It can compensate for the dead-band and saturation of muscle activation characteristics, set the co-stimulation levels to provide stiffness and establish different gains for the muscles in the different operation ranges. It has been shown that co-stimulating muscle can help reject rapid external load disturbances and improve the accuracy of tracking tasks [6,4]. However, the co-stimulation strategy may lead to overall higher stimulation levels, which would cause premature muscle fatigue [2].

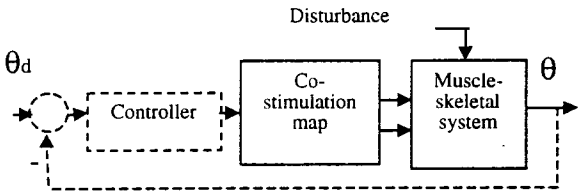

Figure 1. The diagram of a control system. Open loop system shown in solid lines, feedback connection shown in dotted lines.

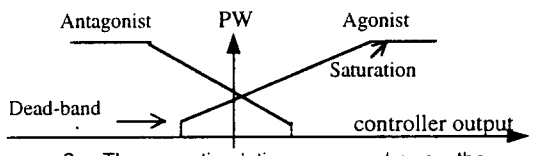

Figure 2. The co-stimulation map shows the relationship between controller output and stimulation level (PW) for each of two muscles.

The goals of this study were to investigate the effects of varying co-stimulation map parameters on control system performance and to determine which system model components had the strongest effects on controller performance.

Methods

- Musculoskeletal Model: The musculoskeletal model we used here was a single skeletal segment inverted pendulum acted upon by a pair of muscles across the joint with one degree-of-freedom [1,5]. Linear joint stiffness and damping acted to resist movement at the joint. The muscles were a modified Hill-type model where active muscle moment is a product of three terms: muscle activation, joint angle factor ($A_{TA}(t)$) and joint angle velocity factor ($A_{TV}(t)$). The muscle activation included third-order recruitment with a dead-band and saturation and discrete-time second-order contraction dynamics. The torque-angle and the torque-velocity relationship are described in Fig 3 and 4. Muscle fatigue was not included in the model. Model parameters were selected to represent the action of hip abductors on the head, arm and trunk (HAT segment).

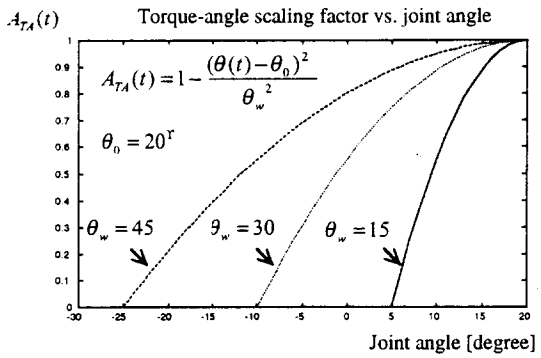

Figure 3. Torque-angle curve of one muscle. Zero degree is the initial joint angle (upright posture). The curve slope varies with θ_w. The results of slope changes were investigated in this study.

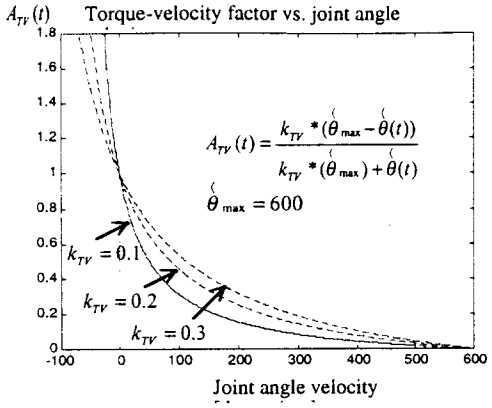

Figure 4. The torque-velocity curve. The curve slope varies with k_{TV}, the effects of changes were investigated in this study.

- Simulation protocols:

Disturbance resistance test: We investigated the role of co-stimulation in providing resistance to disturbances while varying two muscle parameters: θ_w (which affects torque-angle curve slope) and k_{TV} (which affects torque-velocity curve slope) by ±50% of the initial values (30°, 0.2 respectively). A pulse disturbance (amplitude = 8Nm, duration = 2sec) was applied to the system with open-loop control (therefore stimulation values did not change in the trial).

Output tracking test: We investigated the effects of torque-angle width and co-stimulation map intercepts while the control system tried to track two step input in joint angle. A closed-loop PID controller with fixed parameters was used to provide the signal to the PW map (see Fig 1). The values of PID controller parameters were chosen by trial and error and were held constant throughout the study.

Results

Disturbance resistance test

Figure 5 shows the effects of varying model parameters and co-stimulation levels on the peak angular excursion following the disturbance. In the contour plots, the values indicated by the contour represents the peak angle recorded during a trial with a model parameter value (shown on the horizontal axis) and co-stimulation level (shown on the vertical axis).

1. Torque-angle curve slope (θ_w) and co-stimulation level effects

From Figure 5 (a), we see that there is a marked boundary between regions where the system fell and where it returned to upright. Disturbance resistance was highly dependent on the torque-angle model parameter (θ_w), with intermediate values (20-30) providing the best disturbance resistance. Also note that for any given value of θ_w, a certain level of co-stimulation is required to stabilize the system, but further increases may not provide large improvements. For example, for the system of θ_w equal to 25, with co-stimulation set to 21, the system fell; when it was set to 24, the system returned to upright with peak angle equal to 5°; a further increase of co-stimulation level to 27 reduces the peak error only by 1° to 4°. Increasing the co-stimulation level improved the ability to resist the disturbance, but for the system with medium torque-angle curve slope (θ_w), the effects of increase co-stimulation level are not large once a threshold of co-stimulation level is crossed. However, from the plot, we also find that without co-stimulation to a certain level, the disturbance causes the system to fall. For large or small values of θ_w, the co-stimulation level had much larger effects on system response, and a higher co-stimulation level was needed to stabilize the system.

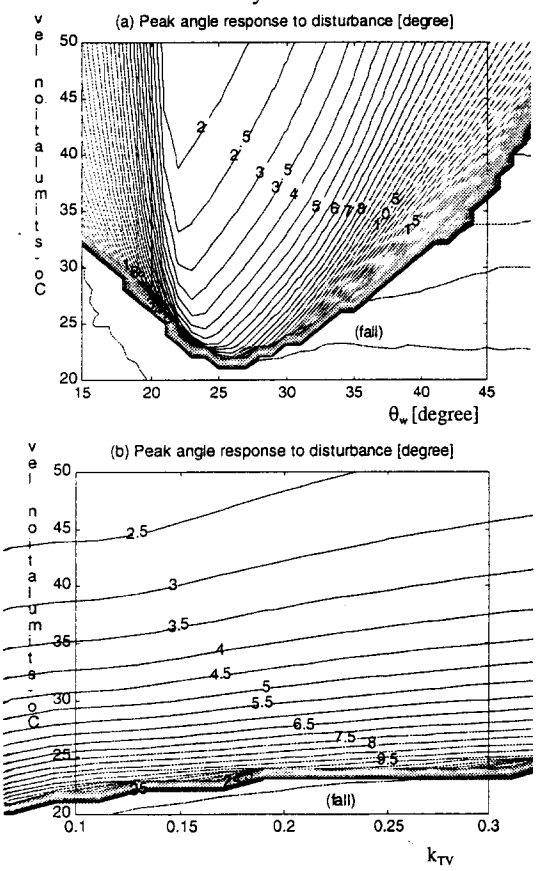

Figure 5. Peak angle responses to a disturbance with co-stimulation intercept changes and the changes of (a) θ_w; (b) k_{TV}.

2. Torque-velocity curve slope (k_{TV}) and co-stimulation level effects

From Figure 5 (b), we find that decreasing k_{TV} increases the curve slope and the system becomes more highly damped. Once again, for a given muscle

parameter value, k_{TV}, a threshold of co-stimulation level must be crossed to provide a stable system response. However, while further increases of co-stimulation provide improvement, the rate of improvement drops off with higher co-stimulation levels.

Output tracking test

Figure 6 shows the response of various systems to a two step input of desired angle. Note that in plot (a), high co-stimulation intercepts increase the stiffness of the system, depress the oscillation, and cause it to respond slowly. From plot (b), we find that torque-angle curve slope (θ_w) has large effects on system response. The systems with steep torque-angle slope (small θ_w) have high stiffness and respond slowly; the systems with shallow torque-angle slope (large θ_w) have low stiffness and exhibit overshoot (dashed line).

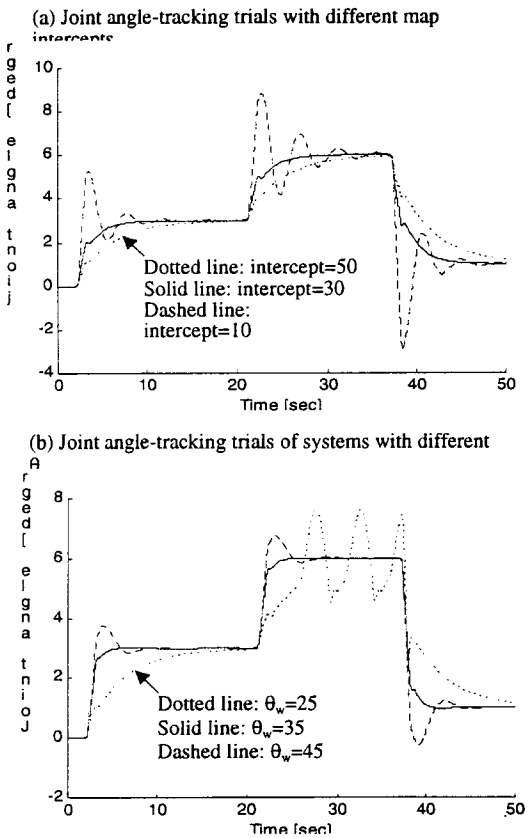

Figure 6. Joint angle-tracking trials while changing (a) co-stimulation map intercepts; (b) θ_w.

Conclusion and Discussion

This study investigated the effects of model parameter values (which cannot be manipulated or easily measured) and co-stimulation map parameters (which are part of the control system that can be tuned). Our results showed that the torque-angle curve slope had a large effect on system performance for the standard disturbance test used here. In contrast, torque-velocity curve slope had a small effect on system performance. Results from the output-tracking test confirmed that control system performance is highly dependent on the muscle torque-angle factor.

The results of the disturbance resistance test showed that for a given musculoskeletal system, a certain co-stimulation level is needed to stabilize the system to a specific disturbance, but that increases of co-stimulation over this level may not substantially improve the system stability. Results from the output tracking test indicated that high co-stimulation intercept increased the stiffness of system and slowed the system response.

The implication of these results for FNS control system development are: (1) the sensitivity to the muscle torque-angle factor (or length-tension curve) should be carefully assessed; (2) increasing co-stimulation level provides diminishing returns, incurs the cost of increased muscle fatigue and may increase control system response time.

Acknowledgements

This work was supported by NIH, Neural Prosthesis Program, #N01-NS-6-2351

References

1. J. J. Abbas and H. J. Chizeck, "Neural Network Control of Functional Neuromuscular Stimulation Systems: Computer Simulation Studies," *IEEE Trans. Biomed. Eng.*, vol. BME-42, pp. 1117-1127
2. P. E. Crago, R. J. Nakai, and H. J. Chizeck, "Feedback Regulation of Hand Grasp Opening and Contact Force During Stimulation of Paralyzed Muscle," *IEEE Trans. Biomed. Eng.*, vol. BME-38, pp. 17-27
3. B. Zhou, S. R. Katz, R. V. Baratta, M. Solomonow and R. D. D'Ambrosia, "Evaluation of Antagonist Coactivation Strategies Elicited from Electrically Stimulated Muscles Under Load-Moving Conditions", *IEEE Trans. Biomed. Eng.*, vol. BME-44, pp. 620-633
4. W. K. Durfee, "Task based methods for evaluation electrically stimulated antagonist muscle controllers", *IEEE Trans. Biomed. Eng.*, vol. BME-36, pp. 309-321
5. D. A. Winter, Biomechanics & Motor Control of Human Movement, 2nd edition, Wiley Pub., 1990, pp. 51-74
6. N. Hogan, "Tuning muscle stiffness can simplify control of natural movement", *1980 ASME Adv. Bioeng.* , pp. 279-282